Efficient synthesis and growth mechanisms of CuO nanowires via self-resistive heating

Thi Ha Tran[1], Nguyen Hai Pham[2], Van Tan Tran[2], Oscar Martínez Sacristán[3], Jyh-Shen Tsay[4], Viet Tuyen Nguyen[2], Van Thanh Pham[2,*]

[1]Hanoi University of Mining and Geology, 18 Vien Street, North Tu Liem, District, Hanoi, Vietnam

[2]Faculty of Physics, Vietnam National University of Science - University of Science Hanoi, 334 Nguyen Trai, Thanh Xuan District, Hanoi, Vietnam

[3]GdS-Optronlab group, Condensed Matter Physics Department, School of Industrial Engineering, University of Valladolid, 47011 Valladolid, Spain.

[4]Department of Physics, National Taiwan Normal University, 162, Section 1, Heping E. Rd., Taipei City 106, Taiwan.

*phamvanthanh@hus.edu.vn (Van Thanh Pham)

Abstract

In this study, we present a fast and facile self-resistive heating method to fabricate copper oxide (CuO) nanowires (NWs) using copper wire substrates. The effect of growth temperature and time were investigated through both experiment and simulations. X-ray diffraction and Raman spectroscopy confirmed the successful formation of highly crystalline CuO phase. Scanning electron microscopy images demonstrated that the NWs were uniform in size and at high density, indicating an efficient synthesis process. Additional analyses were conducted to further elucidate a thermodynamic mechanism of the growth of CuO NWs. Our extensive experimental and simulation data on synthesis parameters provide a detailed view on the growth of the NWs and explain the efficient growth of aligned CuO NWs synthesized by the resistive heating method.

I, Introduction

Cupric oxide (CuO) has garnered significant scientific research interest due to its unique properties and broad potential applications in various scientific fields[1,2]. CuO is a p-type semiconductor with monoclinic structure and a narrow bandgap ranging from 1.2 to 2.1 eV [3,4], making it an ideal material for numerous applications such as photocatalysis [5,6], gas and glucose sensors[7,8], optoelectronics [9,10], field-effect transistors (FETs) [11,12], etc. Notably, CuO also exhibits complex magnetic phases and plays a crucial role in the foundation of several high-temperature superconductors [13,14].

One-dimensional (1D) nanostructures of CuO, including nanowires (NWs) [15,16], nanorods [17], and nanofibers[18], have been synthesized using various methods such as hydrothermal techniques [19], chemical methods [20], electrospinning[21], and thermal oxidation [22]. Among these, the direct thermal oxidation of copper metal has attracted much attention due to its simplicity, efficiency, cost-effectiveness, and scalability [23]. This method is highlight among other thanks to not only facile experimental set up but also higher crystallinity and better uniformity of the nanoproducts. However, the major drawback of traditional thermal oxidation method is the use of high-power-consuming equipment to maintain high temperature in the growth chamber. This not only increases operating costs but also necessitates complex machinery, making rapid production less efficient due to thermal inertia.

In this paper, we report the synthesis of CuO NWs by a novel method, namely, self-resistive heating to address these shortcomings of the traditional thermal oxidation method. Electric current is applied to generate heat directly within the material, offering better temperature control and simplifying the process. Concentrating heat only on a specific area of the sample offers nanostructures with a more uniform size and shape, improving quality at much lower energy consumption and cost. Various characterization techniques such as Scanning Electron Microscopy (SEM), Transmission Electron Microscopy (TEM), Raman spectroscopy, X-ray Diffraction (XRD), and Selected Area Electron Diffraction (SAED), have been employed to understand better the formation, growth processes, and unique properties of these nanostructures. Additionally, simulation was also performed to optimize the fabrication process as well as better understand the growth mechanism. Self-resistive heating approach opens up new avenues for the effective and efficient application and scalable production of metal oxide nanomaterials.

II, Experimental procedure

Cu (99.99%) wires (diameter of 0.25 mm and a length of 90 mm) were ultra sonic treated in a dilute 25% HCl solution for 10 min followed by rinsing thoroughly with acetone and ethanol. Finally, the wires were dried using a nitrogen spraygun. Subsequently, the Cu wires were attached to copper electrodes for resistive heating experiment. A Kikusui Pas10 DC-power supply was utilized to control the current in the samples. The synthesis process was conducted in air ambient.

The structural properties of the obtained material were characterized using a Panalytical Empyrean powder X-ray diffractometer with Cu-Kα radiation ($\lambda = 1.54056$ Å). The morphology and elemental composition of the samples were analyzed using a Nova Nano SEM 450 scanning electron microscope. The morphology as well as the crystallinity of individual CuO NWs was examined with a high-resolution transmission electron microscope (JEM 2100, Joel). Raman spectra of the samples were obtained on a LabRaman 800 spectrometer using a 632.8 nm excitation wavelength. Simulation of the growth conditions of the NWs were performed by finite domain time difference method using Comsol multiphysics software.

III, Results and Discussion

In resistive heating process, heat is generated by the interaction between charged particles and the crystal lattice of the material. The amount of heat that can be released during resistive heating depends on the material's properties, such as density, electrical conductivity, and specific heat capacity. Controlling the amount of heat, or the growth temperature on the sample, is critical to the formation of CuO NWs. Hence, simulation of the temperature on the samples during growth process was performed using COMSOL Multiphysics simulation software.

A 90 mm long copper wire with a diameter of 0.25 mm placed between two electrodes is considered to closely reproduce the practical experimental conditions. The calculation is based on the equation of heat transfer in solids.

$$\rho C_p \frac{\partial T}{\partial t} - \nabla.(k\nabla T) = Q \qquad (1)$$

Where T is the absolute temperature, ρ is the density, C_p is the specific heat capacity at constant stress, Q represents for additional heat sources. In the experiment setup, the addition heat source is the resistive heating due to electrical current, given by:

$$Q = J.E \qquad (2)$$

The electric current density J was set to the identical value used in experiment. Table 1 lists the thermodynamic properties of pure copper used in the simulation.

Table 1. Simulation parameters for simulation of heat transfer in copper material.

Material	Electrical conductivity [S/m]	Heat capacity [J/(kg.K)]	Relative permittivity	Density [kg/m^3]	Thermal conductivity [W/(m.K)]
Copper	5.998.10^7	385	1	8960	400

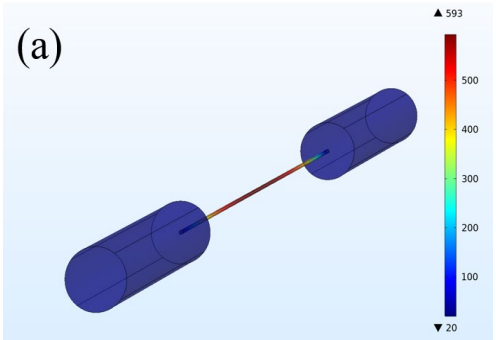

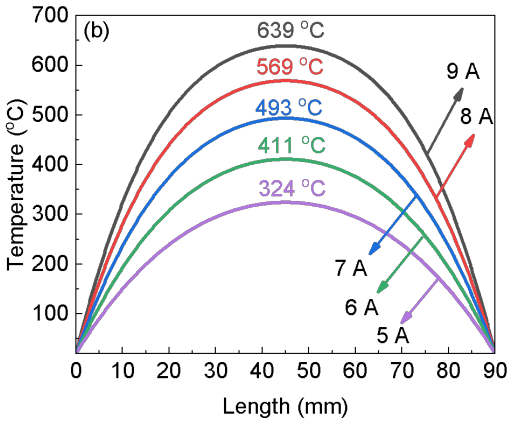

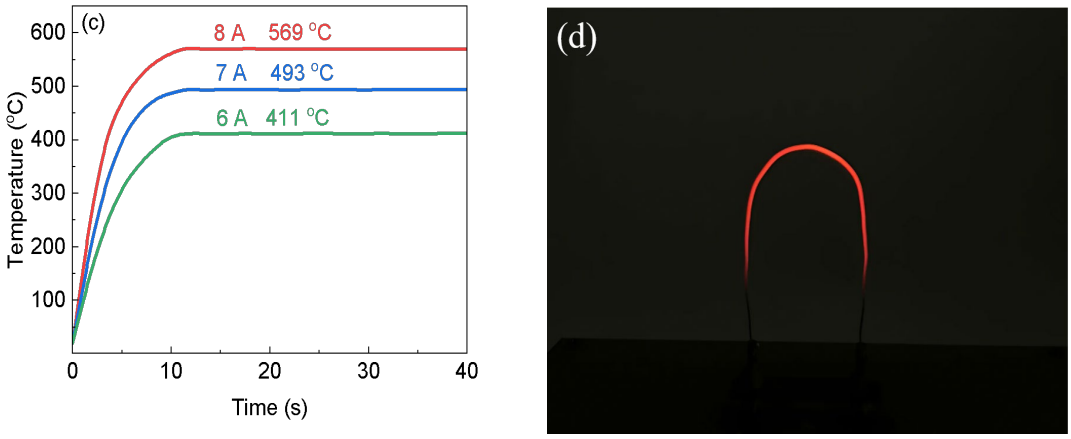

Fig. 1. (a) 3D temperature distribution on the Cu wire annealed with heated by applying a current of 8 A, (b) simulation of temperature along the Cu wire at currents of 5 , 6 , 7 , 8 and 9 A; (c) simulation of dependance of temperature on Cu wire upon time after applying the current
(d) image of a Cu wire during self-resistive heating.

The simulation of the temperature distribution on the copper wire substrates using finite-difference time domain method given in Fig. 1b shows that the peak temperature monotonically increases as raising heating current. The estimated temperatures at the center area of the sample during heating process are 324°C, 411°C, 493°C, 569°C, and 639°C corresponding to the current of 5 A, 6 A, 7A, 8 A, and 9 A, respectively. The simulation data suggest that an uniform temperature was achieved in a region of about 20 mm length in the center of the wire substrate. Previous studies have suggested that the best oxidation temperature for growing CuO NWs is between 400°C and 600°C [24,25]. Hence, the simulation results help to target the appropriate current intensity to achieve designed temperatures for the optimal thermal oxidation growth of CuO nanostructures.

Notably, the temperature simulation also indicates that it takes only about 10 s to reach peak temperature for all the heating currents, demonstrating the efficiency of the resistive heating method. Furthermore, Joule heating exhibits clear advantages compared to other thermal oxidation methods in term of saving energy and cost while minimizing environmental impact. Following the simulation, the experiments were conducted at identical conditions with heating currents of 6 A, 7 A, and 8 A.

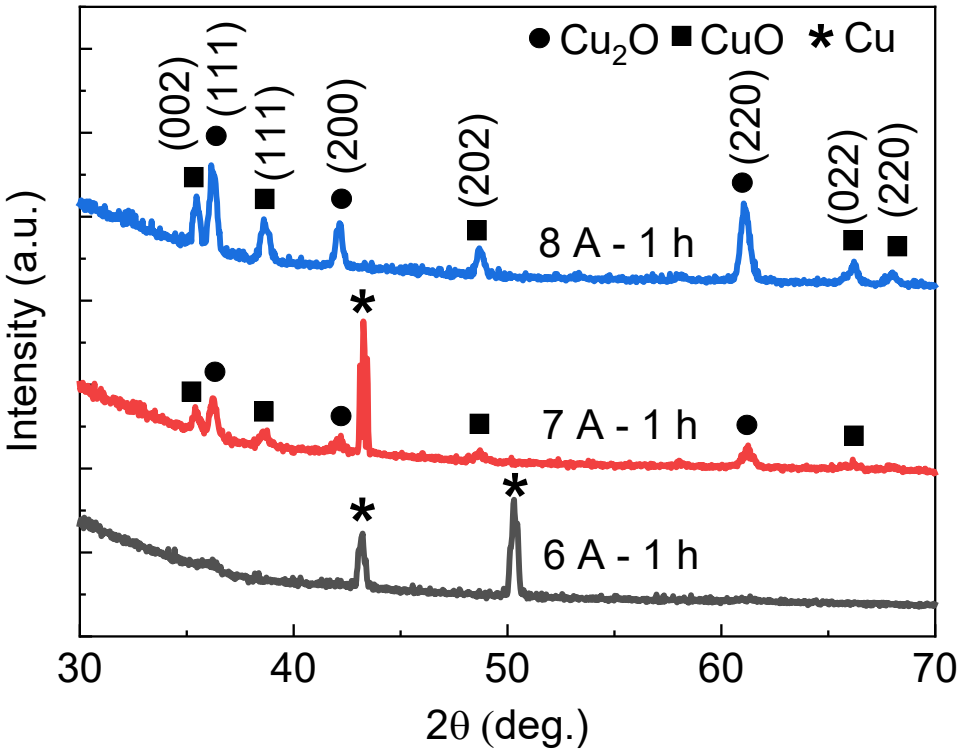

Fig. 2. X-ray diffraction patterns of CuO NWs fabricated in 1 h with current of 6 A, 7 A, and 8 A.

XRD patterns of CuO NW samples fabricated with heating current of 6, 7, and 8 A in 1 h are shown in Figure 2. The XRD pattern of the sample fabricated with a current of 6 A shows only peaks at 43.2° and 50.3° corresponding to copper [26,27]. This indicates that the CuO phase, if present, is too small to be detected by the XRD technique. When the current is increased to 7 A, clear traces of CuO and Cu_2O phases were observed. This result suggests that 7 A is the critical heating current to initiate the oxidation process. When further increasing current to 8 A, the intensity of the diffraction peaks corresponding to copper oxide phases increases significantly while diffraction peaks from Cu phases diminished. This implies the formation of a thick oxide layer on the wire substrate that prevents X-rays signal from the Cu underneath layer. The X-ray diffraction pattern shows distinct Bragg reflections of CuO at 35.4°, 38.7°, 48.7°, and 66.1°, corresponding to the crystal planes (002), (111), (202), (022), and (220) in agreement with the standard JCPDS card 45-0937 of CuO [28,29]. The estimated lattice parameters are a = 4.684 Å, b = 3.425 Å, c = 5.125 Å, and β = 99.549, consistent with the values reported in the literature for CuO materials [30].

Figure 3 illustrates SEM images of NW samples obtained by heating a Cu wire subtrate with different currents. The results demonstrate the obvious impact of heating current on the morphology of the obtained CuO NWs. The SEM image of the sample synthesized at 6 A in Figure 3a clearly shows that the substrates undergo a change in surface morphology. Formation of porous and uneven structures, along with the presence of tiny sparse NWs at early stage was observed. When the current is increased

to 7 A, the obtained CuO NWs become bigger and longer (Figure 3b). However, it can be seen that the growth of NWs is still not complete at this condition. The CuO NWs likely exhibit uniform growth in size and shape when annealing current is set at 8 A.

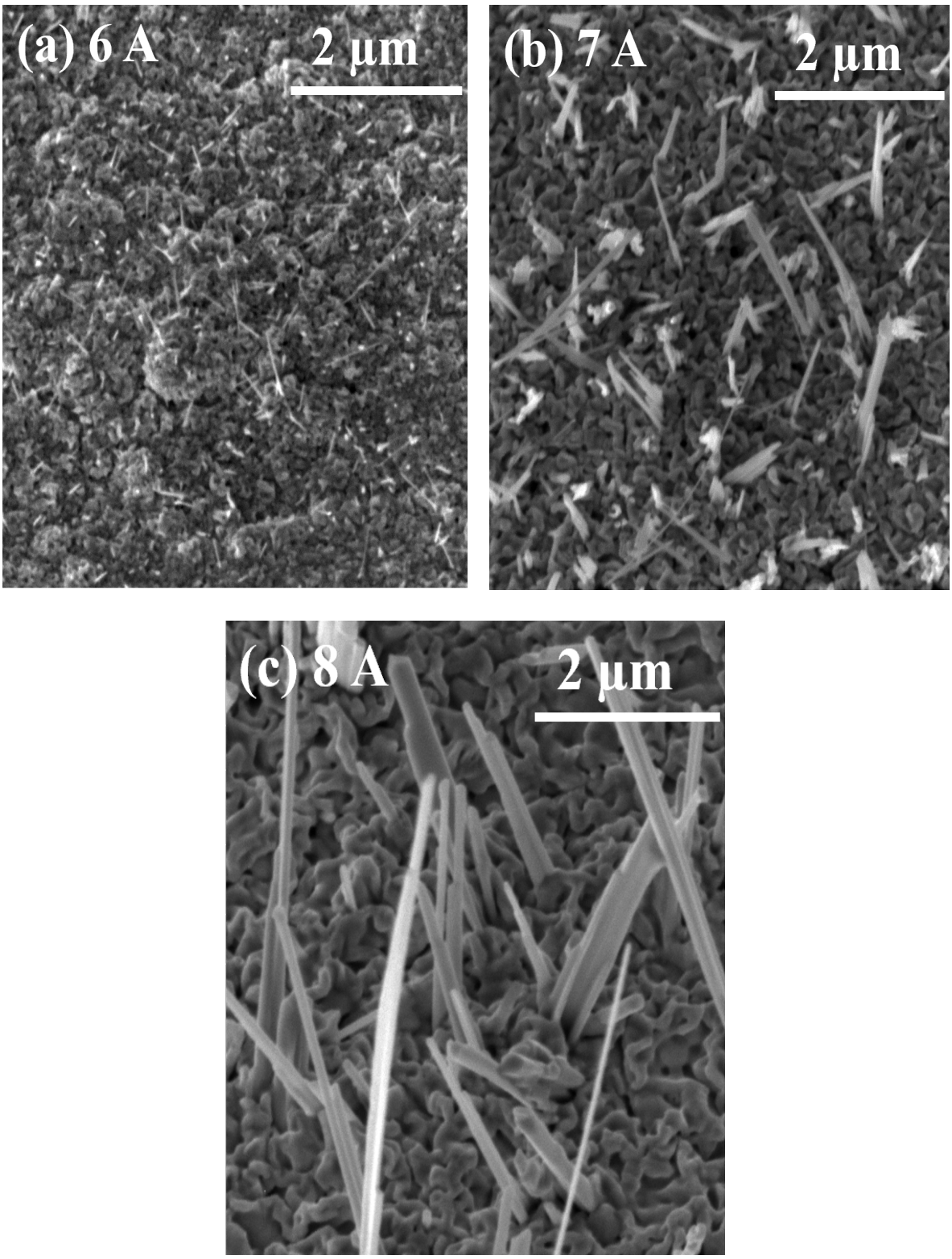

Fig. 3. SEM images of CuO NWs fabricated at different currents: (a) 6 A, (b) 7 A, (c) 8 A.

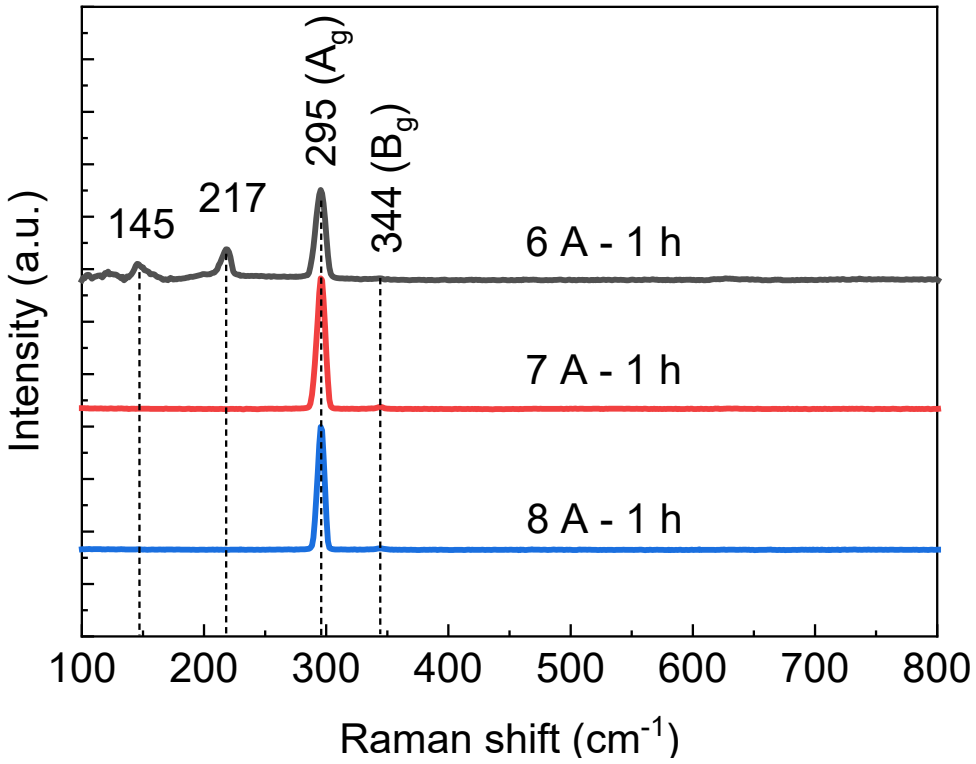

Fig. 4. Raman spectra of CuO NWs fabricated at different currents.

Raman spectra at room temperature of CuO NWs are shown in Fig. 4. Previous studies have shown that the space group of copper oxide C_{2h}^{6} has 12 optical phonon active modes and these modes satisfy $\Gamma_{opt} = 4A_u + 5B_u + A_g + 2B_g$. Among them, A_g and B_g modes are Raman active [31,32]. The CuO NW sample fabricated at 6 A exhibits characterized Raman signals at 295 cm^{-1} and a small peak at 344 cm^{-1} corresponding to the Ag and Bg vibration modes of CuO, respectively [32,33]. In addition to CuO, the presence of the Cu_2O phase in the sample prepared at 6 A is reflected by the presence of features at 145 and 217 cm^{-1} [34]. The noticeable intensity of these modes can be attributed to the relative larger size of Cu_2O grains that formed in the first stage of oxidation [35]. At higher heating current of 7 A and 8 A, Raman peaks of Cu_2O diminished. This is in agreement with the structure transformation shown by XRD measurement discussed above. The investigation with XRD and Raman suggested that heating current of 8 A offers nanoproducts of better crystal quality. It should also be noted that higher current will cause the sample to break during oxidation due to overheating.

The crystal growth process of CuO NWs was further explored by studying the time-dependent nanocrystals growth during the heating process. Therefore, heating current was fixed at 8 A while heating time was increased from 1 to 7 h to observe the effect on structure and morphology of the nanoproducts. SEM images of the CuO NWs formed at different heating times are presented in Figure 5 (a)–(f). At short heating time

of 1, 2 or 3 h, NWs were formed at relatively low density (Figure 5a to c). As the heating time increased to 4 h, the CuO NWs grew significantly longer, reaching several tens of micrometers in length, and their density increased markedly. This suggests that the heating time plays a key role in the formation and growth of CuO NWs.

After 5 h of heating, NWs are formed at the highest density as can be seen in Fig. 5e. Further increasing heating time resulted in no notable change in morphology of the NWs, including diameter, length, and density. This can be understood by the growth mechanism via diffusion of Cu atoms as discussed later.

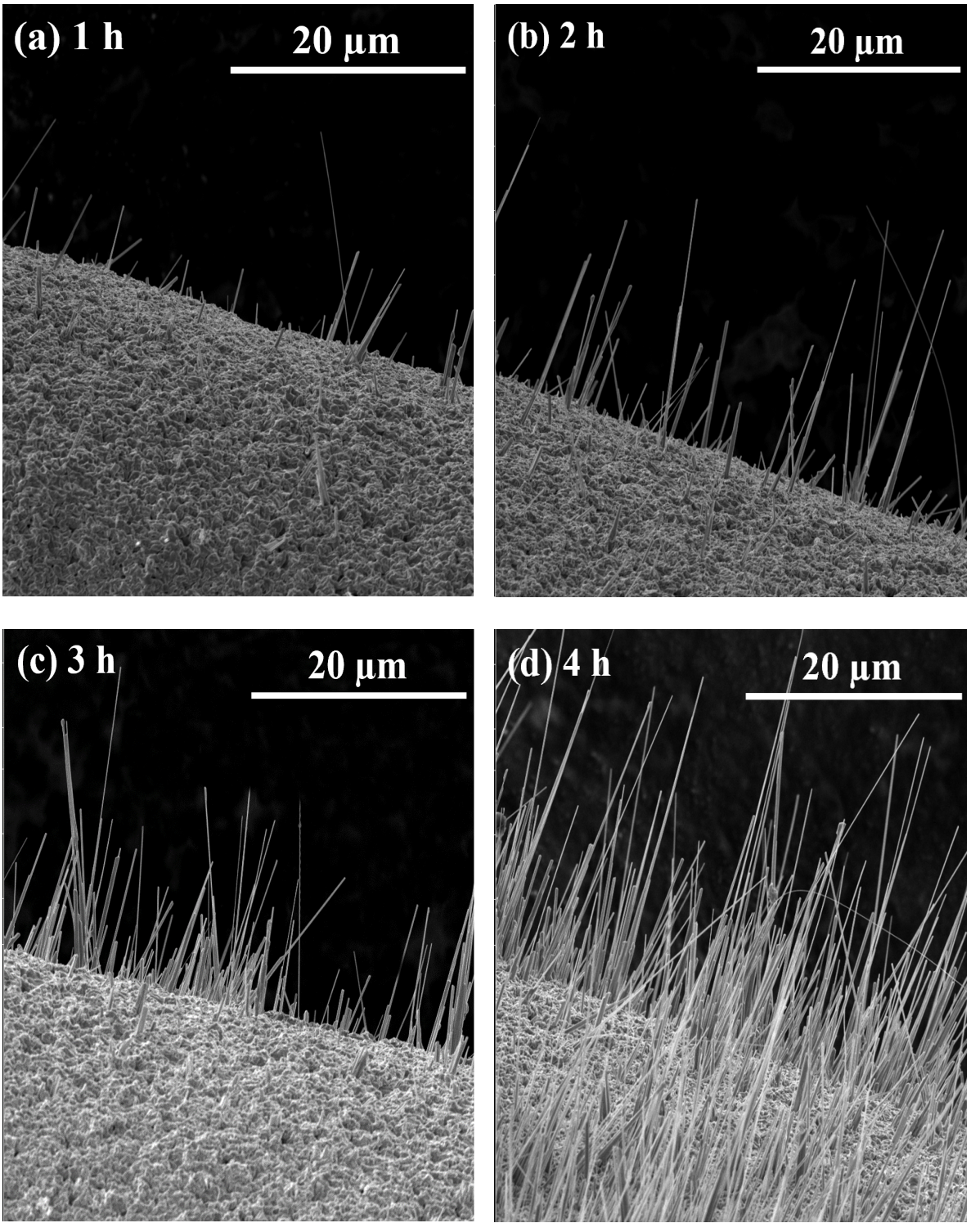

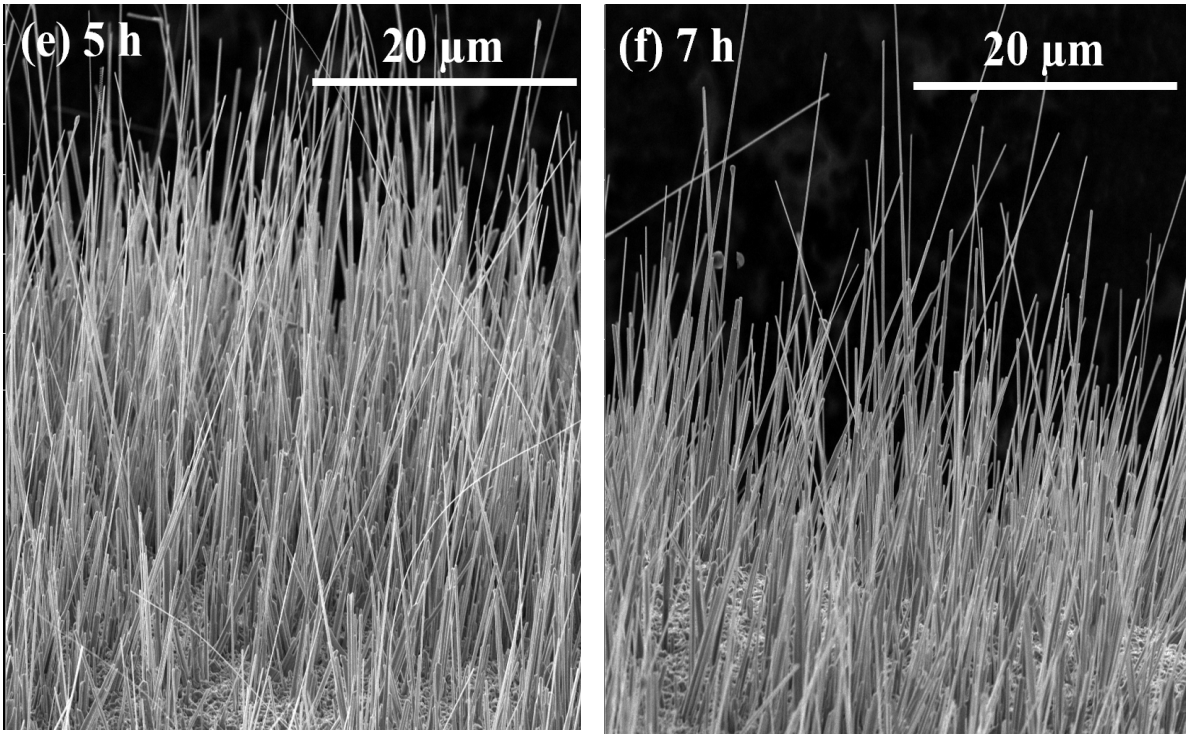

Fig. 5. SEM images of CuO NWs fabricated with a current of 8 A by using different heating times: (a) 1 h, (b) 2 h, (c) 3 h, (d) 4 h, (e) 5 h, (f) 7 h.

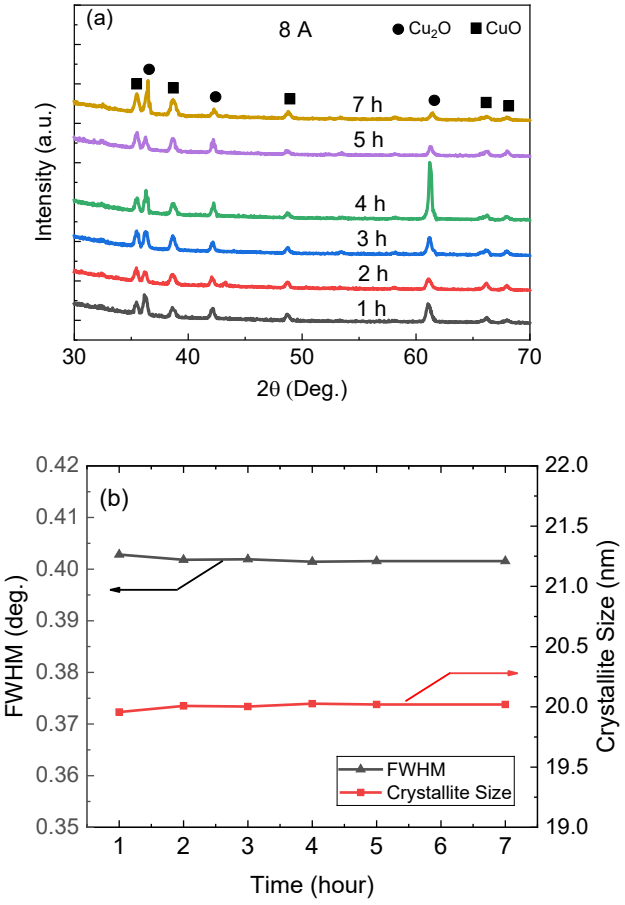

Fig. 6. (a) XRD patterns of CuO NWs fabricated at 8 A with different heating times from 1 to 7 h and (b) FWHM and grain size as a function of annealing time estimated for (002) peak.

The effect of heating time on the phase formation and lattice parameters was analyzed using XRD measurements. Figure 6a shows the XRD patterns of CuO NWs fabricated at 8 A in different annealing time from 1 to 7 h. All diffraction peaks are indexed to CuO (JCPDS card 45-0937) [36]. The crystal size was evaluated by using Scherrer's equation:

$$D_{hkl} = \frac{0.89\lambda}{\beta\, Cos\theta} \quad (1)$$

where D is the crystallite size, λ is the X-ray wavelength (1.54056 Å for Cu-Kα radiation), β is the full width at half maximum (FWHM) of the diffraction peak, and θ is the Bragg angle. The FWHM and crystallite size of CuO NWs estimated for (002) peak as a function of the heating time are shown in Figure 6(b). The results indicate that the crystalline size slightly increased in the first three hours and then remains almost unchanged for longer heating time.

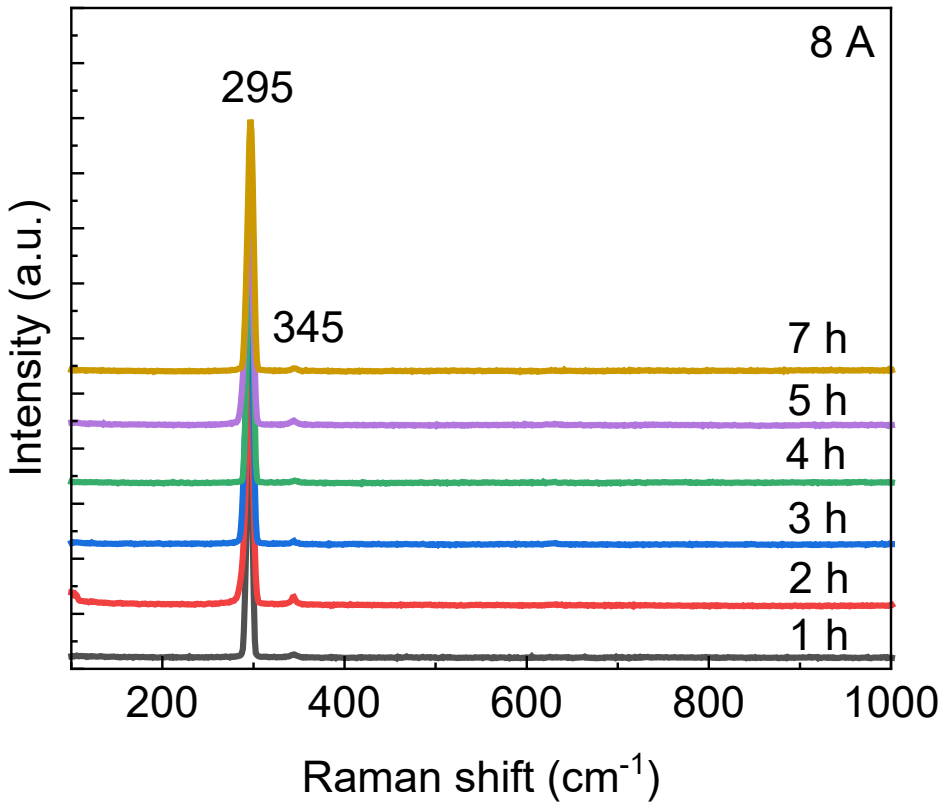

Fig. 7. Raman spectra of CuO NWs fabricated using different heating times from 1 h to 7 h.

The Raman spectra of CuO NWs fabricated at 8 A using different heating times only show the presence of the CuO phase demonstrated by characteristic peaks at 295 cm^{-1} and 344 cm^{-1} (Figure 7) [32]. There is not much difference in the peak positions as well as intensity of the four samples. Thus, it was again shown by Raman spectroscopy that the structure of CuO nanoproducts remained unchanged at all different heating times.

Fig. 8a displays a bright-field TEM image of a single CuO NW fabricated at a current of 8 A in 5 h. Fig. 8b shows the corresponding SAED pattern. The TEM image evidences a smooth and clean surface, cylindrical shape, and a diameter of 65 nm. The lattice planes obtained from the corresponding SAED pattern (Fig. 8b) are consistent with the single-phase monoclinic crystal structure of CuO [37].

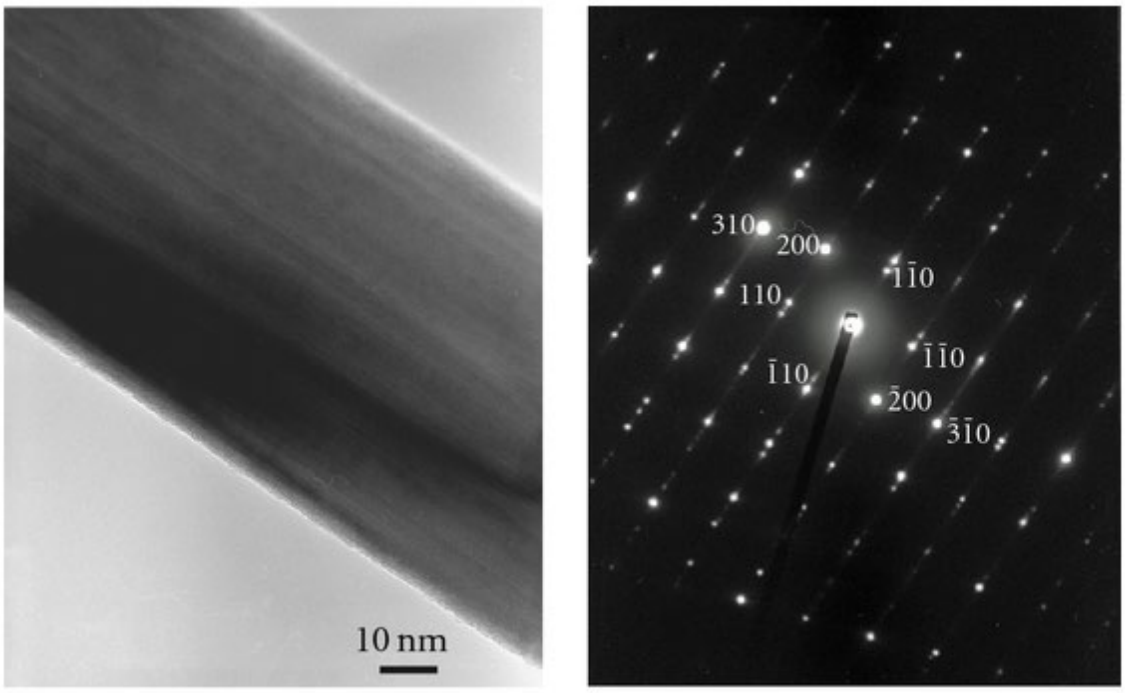

(a) (b)

Fig. 8. (a) Bright-field TEM image of a single CuO NW (b) The corresponding SAED pattern.

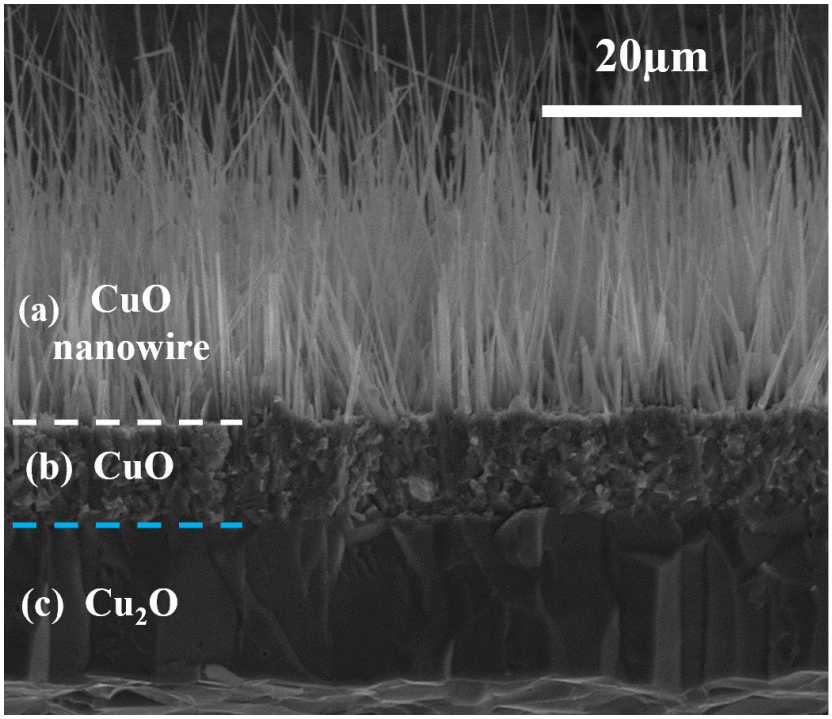

Fig. 9. Cross-sectional SEM image of CuO NW sample prepared at 8 A in 5h.

The cross-sectional SEM image of NWs fabricated at 8 A in 5 h is shown in Fig. 9. The formation of three distinct layers on the wire substrate is clearly seen. The surface layer consists of long CuO NWs with lengths of several tens of micrometers. The underneath layer from surface is a layer with a thickness of approximately 6 to 8 micrometers, consisted of small grains. The bottom layer is composed of larger grains with grain size of several micrometers.

The EDS spectra obtained from the top layer (a), the intermediate layer (b), and the bottom layer (c) of the oxide wire are shown in Figures 10 (a), (b), and (c), respectively. The results indicate that the elemental ratio of Cu to O of the bottom layer is very different from that of the other two layers on top . It is evident that the elemental ratio of Cu to O in layer (a) is approximately 2:1 while this ratio is almost 1: 1 for the other two layers.

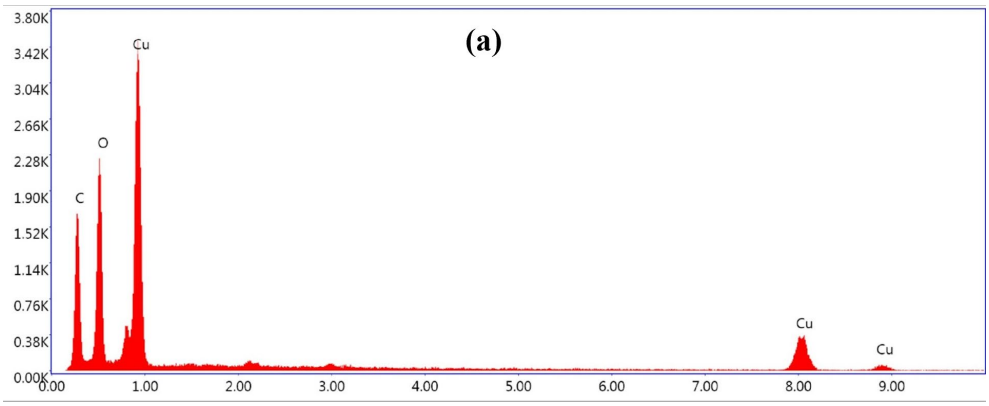

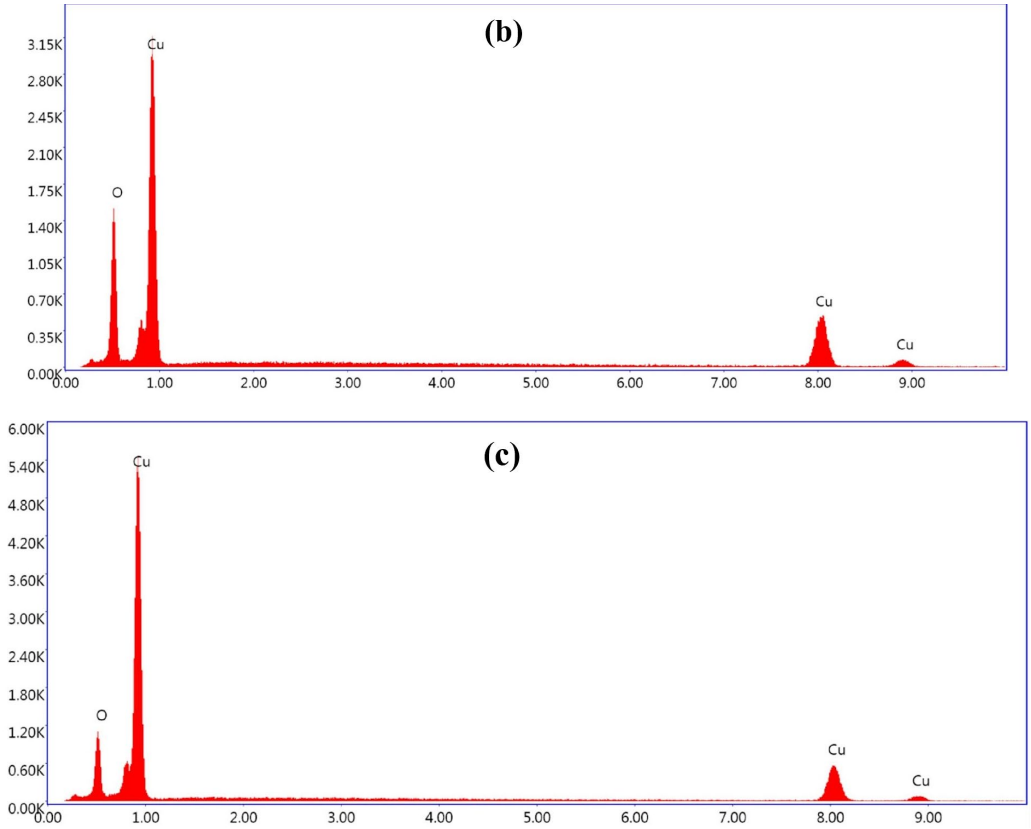

Fig. 10. EDS spectra of (a) top surface of CuO NW, (b) CuO layer, (c) Cu_2O layer

Our previous study has proposed that the diffusion of Cu ions through grain boundaries is the primary mechanism explaining the growth of CuO NW structures during the oxidation of the Cu wire substrate [38,39]. In this research, we also believe that the growth mechanism of CuO NWs fabricated using the Joule heating method is attributed to diffusion of Cu ions. It is noted that the NWs prepared by resistive heating are likely formed at higher densities compared with traditional heating method using horizontal furnaces. We believed that in the resistive heating process, two effects are responsible for the high yield formation of aligned CuO NWs. Firstly, heat is effectively generated in the local region of the copper wires used as substrates when an electric current is applied. Secondly, the electromigration effect, which involves the diffusion of metal atoms under high current densities in the direction of the electron flow also support for the growth rate and efficiency of the oxidation process [40]. The development of CuO NWs is illustrated schematically in Fig. 11.

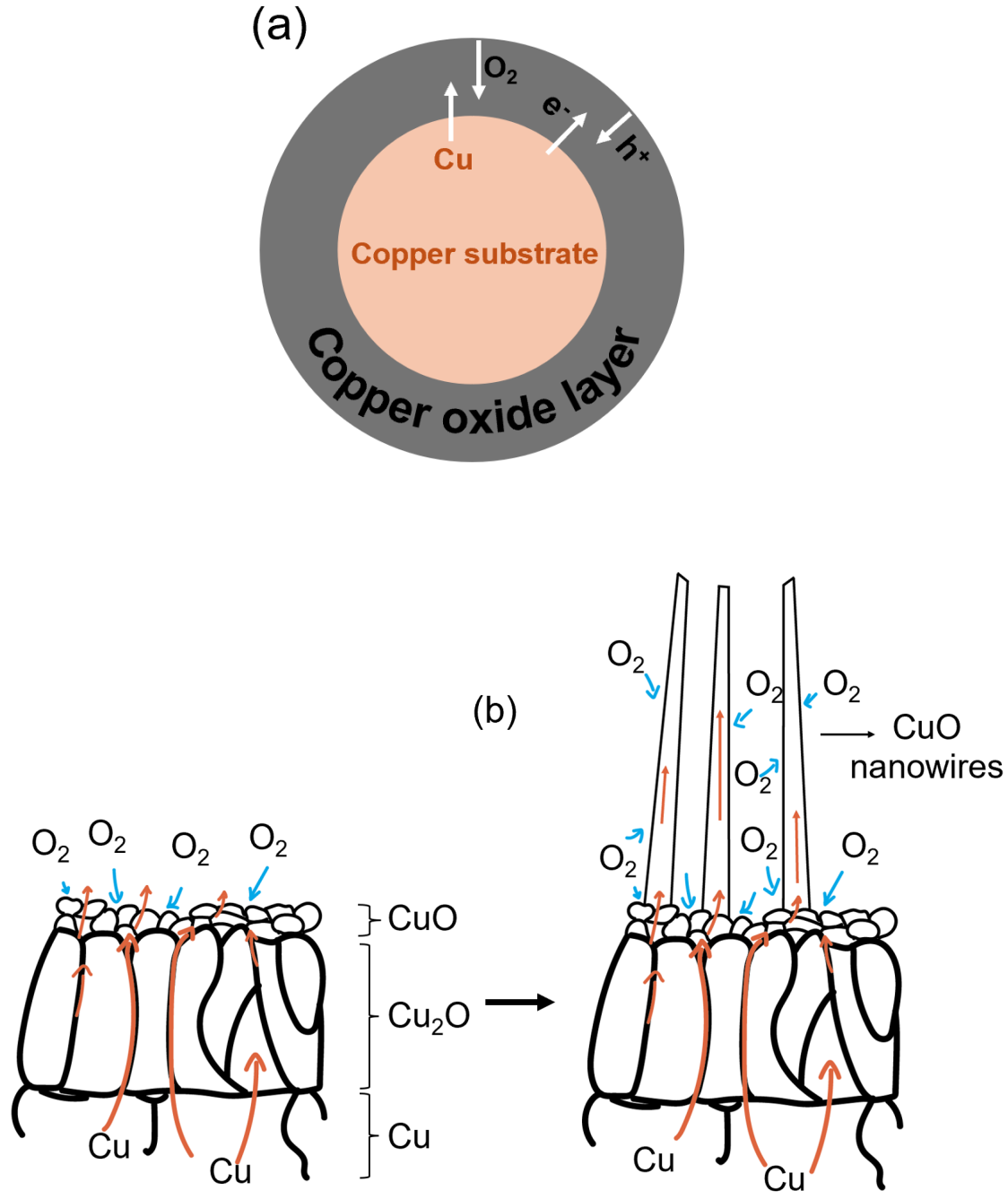

Fig. 11. Schematic diagram of (a) the cross-sectional view of the oxidation of the wire sample at the first stage, and (b) illustration of the growth of CuO NWs at the second stage.

In the initial stage, the Joule heating process generates thermal expansion within the crystal lattice. This process creates a temperature gradient from the core of the copper wire substrate to the outer surface, significantly impacting the diffusion of copper atoms [41]. As the temperature rises, copper atom diffusion accelerates, promoting faster electromigration. The rapid diffusion of copper atoms through grain

boundaries and along the crystal lattice to the surface, combined with the counter-diffusion of oxygen atoms, leads to the formation of a Cu_2O layer. As the heating time increases, this layer thickens and eventually transforms into CuO on the surface. In parallel, the presence of an electric field enhances the growth of CuO NWs, accelerating the growth rate and resulting in longer NW lengths.

Subsequently, copper atoms continue to diffuse from the copper substrate to the copper oxide layers, resulting in the formation of CuO NWs. Compressive stress at the surface of the Cu_2O and CuO layers drives the outward diffusion of copper atoms through grain boundaries, providing a continuous supply of Cu ions for the growth of CuO NWs. The driving force for copper diffusion is the applied current density during the heating process. If the applied current is low, it results in low thermal oxidation temperature and insufficient compressive stress to promote the growth of CuO NW structures. Instead, deformed Cu_2O particles form on the substrate surface to relieve the minor compressive stress. At higher heating currents, copper atoms diffuse through grain boundaries much more rapidly than through the crystal lattice. The efficient growth of CuO NWs observed in this study can also be explained by a diffusion process of the oxygen inside the metal that is accelerated by electromigration at the high electrical currents employed. Furthermore, even at optimal heating current values, the density and growth of CuO NWs vary over time. This indicates that sufficient time is needed for stress to accumulate to the critical point for CuO NW growth. This explain the low density of NWs obtained at low current or short heating times, as observed. As oxidation time increases and the copper oxide layers thicken, the development of CuO NWs is restricted because it is more challenging for Cu atoms to diffuse a long distance to the tips of the CuO NWs. At the same time, the continuous growth of a CuO layer just beneath the NWs tends to merge the root of the NWs, which appear as a reduction in the length and density of the CuO NW substrates for prolonged heating.

IV, Conclusion

We present a detailed study of the growth of CuO NWs using a simple and rapid self-resistive heating method applied to copper substrates under ambient air conditions. Our results demonstrate the influence of the applied current and heating time on the structural and morphological characteristics of the CuO NWs. At optimum condition, where the samples were heated by a current of 8 A in 5h, densely packed CuO NWs of uniform size and shape were obtained. The growth mechanism involves the diffusion of copper atoms across grain boundaries and the inward-diffusion of oxygen from the environment. Both diffusion processes are accelerated by Joule heating. In addition, the electromigration effect plays an important role in the diffusion of copper atoms at high current densities, which further enhances the NW formation process. These findings provide valuable insights into the fabrication and growth mechanism of CuO NWs, highlighting the efficiency and potential of the self-resistive heating method for producing high-quality nanostructures.

Acknowledgement:

This research is funded by Vietnam National Foundation for Science and Technology Development (NAFOSTED) under grant number 103.99–2020.33.

References

[1] U. Sidiqi, M. Ubaidullah, A. Kumar, D. Kumar, K. Muzammil, M. Imran, Progress on cupric oxide based nanomaterials: Exploring advancements in their synthesis, applications and prospects, Materials Science and Engineering: B 308 (2024) 117598. https://doi.org/10.1016/J.MSEB.2024.117598.

[2] T.H. Tran, T.M.A. Nguyen, V.P.T. Dao, C.D. Sai, T.C. Bach, N.H. Pham, A.B. Ngac, V.T. Pham, T.K.C. Tran, H. Cheong, V.T. Nguyen, Highly sensitive characteristic of surface enhanced Raman scattering for CuO/Au core/shell nanowires substrate, Ceram Int 48 (2022) 3199–3205. https://doi.org/10.1016/J.CERAMINT.2021.10.093.

[3] A. Mahmood, F. Tezcan, G. Kardaş, Photoelectrochemical characteristics of CuO films with different electrodeposition time, Int J Hydrogen Energy 42 (2017) 23268–23275. https://doi.org/10.1016/J.IJHYDENE.2017.06.003.

[4] M. Balık, V. Bulut, I.Y. Erdogan, Optical, structural and phase transition properties of Cu2O, CuO and Cu2O/CuO: Their photoelectrochemical sensor applications, Int J Hydrogen Energy 44 (2019) 18744–18755. https://doi.org/10.1016/J.IJHYDENE.2018.08.159.

[5] H.T. Berede, D.M. Andoshe, N.S. Gultom, D.H. Kuo, X. Chen, H. Abdullah, T.H. Wondimu, Y. nan Wu, O.A. Zelekew, Photocatalytic activity of the biogenic mediated green synthesized CuO nanoparticles confined into MgAl LDH matrix, Scientific Reports 2024 14:1 14 (2024) 1–13. https://doi.org/10.1038/s41598-024-52547-w.

[6] A.K. Sibhatu, G.K. Weldegebrieal, S. Sagadevan, N.N. Tran, V. Hessel, Photocatalytic activity of CuO nanoparticles for organic and inorganic pollutants removal in wastewater remediation, Chemosphere 300 (2022) 134623. https://doi.org/10.1016/J.CHEMOSPHERE.2022.134623.

[7] A. Umar, A.A. Alshahrani, H. Algarni, R. Kumar, CuO nanosheets as potential scaffolds for gas sensing applications, Sens Actuators B Chem 250 (2017) 24–31. https://doi.org/10.1016/J.SNB.2017.04.062.

[8] A. Ashok, A. Kumar, F. Tarlochan, Highly efficient nonenzymatic glucose sensors based on CuO nanoparticles, Appl Surf Sci 481 (2019) 712–722. https://doi.org/10.1016/J.APSUSC.2019.03.157.

[9] H.M. Alhusaiki Alghamdi, Structural, morphological, optical, and electrical characteristics of polyethylene oxide/ chitosan-copper oxide nanoparticles for optoelectronic applications, Opt Mater (Amst) 134 (2022) 113101. https://doi.org/10.1016/J.OPTMAT.2022.113101.

[10] M.A.M. Patwary, M.A. Hossain, B.C. Ghos, J. Chakrabarty, S.R. Haque, S.A. Rupa, J. Uddin, T. Tanaka, Copper oxide nanostructured thin films processed by SILAR for optoelectronic applications, RSC Adv 12 (2022) 32853–32884. https://doi.org/10.1039/D2RA06303D.

[11] A.K. Mishra, D.K. Jarwal, B. Mukherjee, A. Kumar, S. Ratan, S. Jit, CuO Nanowire-Based Extended-Gate Field-Effect-Transistor (FET) for pH Sensing and Enzyme-Free/Receptor-Free Glucose Sensing Applications, IEEE Sens J 20 (2020) 5039–5047. https://doi.org/10.1109/JSEN.2020.2966585.

[12] H. Zhu, A. Liu, G. Liu, F. Shan, Electrospun p-type CuO nanofibers for low-voltage field-effect transistors, Appl Phys Lett 111 (2017). https://doi.org/10.1063/1.4998787/34092.

[13] A.K. Tyagi, S. Tyagi, T.P. Sharma, About the substitutions for CuO in YBCO high temperature superconductor, Materials Science and Engineering: B 45 (1997) 88–97. https://doi.org/10.1016/S0921-5107(96)01912-5.

[14] T. Ito, H. Takagi, S. Ishibashi, T. Ido, S. Uchida, Normal-state conductivity between CuO2 planes in copper oxide superconductors, Nature 1991 350:6319 350 (1991) 596–598. https://doi.org/10.1038/350596a0.

[15] G. Fritz-Popovski, F. Sosada-Ludwikowska, A. Köck, J. Keckes, G.A. Maier, Study of CuO Nanowire Growth on Different Copper Surfaces, Scientific Reports 2019 9:1 9 (2019) 1–13. https://doi.org/10.1038/s41598-018-37172-8.

[16] R. Siddaramaiah, V. Kumar Singh Yadav, A. Pal, R. Paily Palathinkal, High-performance CuO nanowire printed devices for visible light sensing and switching characteristics, Mater Lett 320 (2022) 132300. https://doi.org/10.1016/J.MATLET.2022.132300.

[17] X. Chen, S. Huang, Z. Zhang, L. Qiu, F. Liu, T. Liu, Y. Ouyang, Y. Shen, In-situ growth of CuO nanorods on sensing electrodes and their gas sensing properties of VOCs, Ceram Int (2024). https://doi.org/10.1016/J.CERAMINT.2024.09.336.

[18] A.P. Dantas, R.A. Raimundo, P.F.C. Neto, C.M.S. Lopes, J.R.D. Santos, F.J.A. Loureiro, T.O. Pereira, M.A. Morales, E.S. Medeiros, D.A. Macedo, Copper oxide nanofibers obtained by solution blow spinning as catalysts for oxygen evolution reaction, Ceram Int 50 (2024) 13034–13045. https://doi.org/10.1016/J.CERAMINT.2024.01.213.

[19] T. Jiang, Y. Wang, D. Meng, X. Wu, J. Wang, J. Chen, Controllable fabrication of CuO nanostructure by hydrothermal method and its properties, Appl Surf Sci 311 (2014) 602–608. https://doi.org/10.1016/J.APSUSC.2014.05.116.

[20] V. Sumalatha, D. Ayodhya, Fabrication and characterization of CuO nano-needles from thermal decomposition of Cu(II) metal complex: Fluorometric detection of antibiotics, antioxidant, and antimicrobial activities, Results Chem 5 (2023) 100821. https://doi.org/10.1016/J.RECHEM.2023.100821.

[21] F.H. Alshafei, D.A. Simonetti, Targeted morphology of copper oxide based electrospun nanofibers, Chem Eng Sci 219 (2020) 115547. https://doi.org/10.1016/J.CES.2020.115547.

[22] D. Mahana, A.K. Mauraya, P. Singh, S.K. Muthusamy, Evolution of CuO thin films through thermal oxidation of Cu films prepared by physical vapour deposition techniques, Solid State Commun 366–367 (2023) 115152. https://doi.org/10.1016/J.SSC.2023.115152.

[23] F. Li, X. Tan, D. Flock, R. Qiu, D. Wang, P. Schaaf, Formation of CuO whiskers and facet-controlled oxidation during the oxidation of Au-Cu nanoparticles fabricated by solid-state dewetting, Appl Surf Sci 610 (2023) 155547. https://doi.org/10.1016/J.APSUSC.2022.155547.

[24] L. Xiang, J. Guo, C. Wu, M. Cai, X. Zhou, N. Zhang, A brief review on the growth mechanism of CuO nanowires via thermal oxidation, J Mater Res 33 (2018) 2264–2280. https://doi.org/10.1557/JMR.2018.215/METRICS.

[25] W. Wang, Y. Zhuang, L. Li, Structure and size effect of CuO nanowires prepared by low temperature solid-phase process, Mater Lett 62 (2008) 1724–1726. https://doi.org/10.1016/J.MATLET.2007.09.086.

[26] N. V. Suramwar, S.R. Thakare, N.T. Khaty, One pot synthesis of copper nanoparticles at room temperature and its catalytic activity, Arabian Journal of Chemistry 9 (2016) S1807–S1812. https://doi.org/10.1016/J.ARABJC.2012.04.034.

[27] B. Bagchi, P. Datta, C.S. Fernandez, P. Gupta, S. Jaufuraully, A.L. David, D. Siassakos, A. Desjardins, M.K. Tiwari, Flexible triboelectric nanogenerators using transparent copper nanowire electrodes: energy harvesting, sensing human activities and material recognition, Mater Horiz 10 (2023) 3124–3134. https://doi.org/10.1039/D3MH00404J.

[28] D. Deng, J. Zheng, X. Chen, W. Sun, Fabrication and Characterization of CuO nanowires on V-shaped Microgroove surfaces, Current Applied Physics 28 (2021) 26–34. https://doi.org/10.1016/J.CAP.2021.04.026.

[29] D. Zhu, L. Wang, W. Yu, H. Xie, Intriguingly high thermal conductivity increment for CuO nanowires contained nanofluids with low viscosity,

Scientific Reports 2018 8:1 8 (2018) 1–12. https://doi.org/10.1038/s41598-018-23174-z.

[30] M.H. Chou, S.B. Liu, C.Y. Huang, S.Y. Wu, C.L. Cheng, Confocal Raman spectroscopic mapping studies on a single CuO nanowire, Appl Surf Sci 254 (2008) 7539–7543. https://doi.org/10.1016/J.APSUSC.2007.12.065.

[31] A.S. Zoolfakar, R.A. Rani, A.J. Morfa, A.P. O'Mullane, K. Kalantar-Zadeh, Nanostructured copper oxide semiconductors: a perspective on materials, synthesis methods and applications, J Mater Chem C Mater 2 (2014) 5247–5270. https://doi.org/10.1039/C4TC00345D.

[32] T.H. Tran, V.T. Nguyen, Copper Oxide Nanomaterials Prepared by Solution Methods, Some Properties, and Potential Applications: A Brief Review, Int Sch Res Notices 2014 (2014) 856592. https://doi.org/10.1155/2014/856592.

[33] F.A. Akgul, G. Akgul, N. Yildirim, H.E. Unalan, R. Turan, Influence of thermal annealing on microstructural, morphological, optical properties and surface electronic structure of copper oxide thin films, Mater Chem Phys 147 (2014) 987–995. https://doi.org/10.1016/J.MATCHEMPHYS.2014.06.047.

[34] R.D. Prabu, S. Valanarasu, I. Kulandaisamy, V. Ganesh, M. Shkir, A. Kathalingam, Studies on copper oxide thin films prepared by simple nebulizer spray technique, Journal of Materials Science: Materials in Electronics 28 (2017) 6754–6762. https://doi.org/10.1007/S10854-017-6371-2/METRICS.

[35] Y. Unutulmazsoy, C. Cancellieri, L. Lin, L.P.H. Jeurgens, Reduction of thermally grown single-phase CuO and Cu2O thin films by in-situ time-resolved XRD, Appl Surf Sci 588 (2022) 152896. https://doi.org/10.1016/J.APSUSC.2022.152896.

[36] X. Zeng, M. Zhukova, S. Faniel, J. Proost, D. Flandre, Structural and Opto-electronic characterization of CuO thin films prepared by DC reactive magnetron sputtering, Journal of Materials Science: Materials in Electronics 31 (2020) 4563–4573. https://doi.org/10.1007/S10854-020-03007-4/METRICS.

[37] D. Su, X. Xie, S. Dou, G. Wang, CuO single crystal with exposed {001} facets - A highly efficient material for gas sensing and Li-ion battery applications, Scientific Reports 2014 4:1 4 (2014) 1–9. https://doi.org/10.1038/srep05753.

[38] J. Shi, L. Qiao, Y. Zhao, Z. Sun, W. Feng, Z. Zhang, J. Wang, X. Men, Synergistic effects on thermal growth of CuO nanowires, J Alloys Compd 815 (2020) 152355. https://doi.org/10.1016/J.JALLCOM.2019.152355.

[39] G. Fritz-Popovski, F. Sosada-Ludwikowska, A. Köck, J. Keckes, G.A. Maier, Study of CuO Nanowire Growth on Different Copper Surfaces, Scientific Reports 2019 9:1 9 (2019) 1–13. https://doi.org/10.1038/s41598-018-37172-8.

[40] S.K. Lin, Y.C. Liu, S.J. Chiu, Y.T. Liu, H.Y. Lee, The electromigration effect revisited: non-uniform local tensile stress-driven diffusion, Scientific Reports 2017 7:1 7 (2017) 1–10. https://doi.org/10.1038/s41598-017-03324-5.

[41] P. Salev, E. Kisiel, D. Sasaki, B. Gunn, W. He, M. Feng, J. Li, N. Tamura, I. Poudyal, Z. Islam, Y. Takamura, A. Frano, I.K. Schuller, Local strain inhomogeneities during electrical triggering of a metal–insulator transition revealed by X-ray microscopy, Proc Natl Acad Sci U S A 121 (2024) e2317944121. https://doi.org/10.1073/PNAS.2317944121/SUPPL_FILE/PNAS.2317944121.SAPP.PDF.